MPC-based Double-layer Real-time Conditional Self-restoration for Interconnected Microgrids

[1]Hongji Hu, [2,*]Samson S. Yu, [3]Junbo Zhao, [4]Tatkei Chau, [5]Fei Ding, [4]Tyrone Fernando, [2]Hieu Trinh

[*] *Corresponding author: s.yu@ieee.org.*

[1] *Department of Electrical and Electronic Engineering, University of Melbourne, Parkville, Victoria, 3010, Australia.*

[2,*] *School of Engineering, Deakin University, 75 Pigdons Rd, Waurn Ponds, Victoria, 3216, Australia.*

[3] *Department of Electrical and Computer Engineering, Mississippi State University, 75 B. S. Hood Road, MS 39762, USA.*

[4] *School of Engineering, University of Western Australia, 35 Stirling Hwy, Crawley, WA 6009, Australia.*

[5] *National Renewable Energy Laboratory, 15013 Denver West Parkway Golden, CO, USA.*

Abstract

2.1 In this work, we propose a novel model predictive control (MPC)-based real-time conditional self-restoration energy management system (CSR-EMS) for interconnected microgrids (IMGs) integrated with renewable energy sources (RESs) and energy storage systems (ESSs). Superior to the existing IMG self-restoration methods, the "conditionality" of the proposed CSR-EMS can economically realize self-restoration and grid-assisted restoration during energy deficiency or faults, in both islanded and grid-connected modes. Cost minimization is implemented as the objective function to judge in real-time which restoration mode is economically preferred. The proposed CSR-EMS comprises two layers– the lower layer operates locally to eliminate electricity fluctuations created by RESs and ensure economic effectiveness within an MG, whereas the upper layer oversees the real-time operational status of the IMG system and determines power exchange among microgrids (MGs) during abnormalities. In detail, when a microgrid inside the IMG system experiences an energy deficiency, the CSR-EMS, on an MPC basis, intelligently optimizes power production from each

dispatchable distributed generator (DG), ESS, power imported from the main grid, and power exchange among the IMGs to maintain the demand-supply balance, while considering system recovery cost, state of charge (SoC) of ESSs and operation modes of the IMGs (i.e., grid-connected or islanded mode). Simulation results and comparisons with existing IMG self-healing EMSs demonstrate the economic efficacy of the proposed CSR-EMS strategy during normal and abnormal operations, which can be used as an energy control framework for modern power systems with multiple interconnected microgrids.

Keywords: Model predictive control, conditional microgrid self-restoration, interconnected microgrids.

---

1. Introduction

It is expected that renewable energy will account for 50% of Australia's total energy by 2025 [1]. Currently, a burgeoning number of microgrids (MGs) consisting of distributed generators, such as wind and solar photovoltaic (PV) energy systems, backup diesel generators, energy storage systems, and controllable loads, are being formed across the country. The key to stable and economic operations of such systems is developing an effective energy management system (EMS) to cope with a variety of operating modes, e.g. islanded and unification modes [2]. Due to forecast errors of uncertain RESs, uncertainty in MGs has become a major issue. According to *IEEE Standard 1547.4* [3], the performance of islanded power systems can be improved by interconnecting them, so as to compensate each other's energy fluctuation and deficiency. In particular, IMGs can contribute to black-start support, better utilization of distributed energy resources (DERs) and attenuation of interferences caused by intermittent wind and solar energy [4], thus enhancing reliability and resiliency of the IMGs.

Normally, the overall EMS of an IMG system is executed by a distribution system operator (DSO), with which the entire EMS is processed in two layers, i.e. MG-control layer and IMG-control layer with the tertiary control that regulates the power flowing to the point of common coupling [5, 6]. In case of extreme

events, each MG is encouraged to be disconnected from the main grid to avoid being affected by serious blackouts [7], which however bears technical difficulty and requires excessive DER capacities for peak demands.

Researches have shown reliability and economic efficiency of interconnected MGs. In [8, 9], a black-out scenario is incorporated in IMGs and an EMS is designed to enable two MGs to work synergistically to support all non-controllable loads in an islanded IMG system without scheduling the power exchange between MGs. Some other research work has been conducted on economic dispatch for grid-connected IMGs [10, 11, 12]. In detail, priority-based EMS for IMGs was proposed in [10], where each MG is encouraged to share energy with other MGs rather than import electricity from the main grid. But the proposed EMS does not consider the regular change of electricity price. In [11], the condition when an MG may simultaneously import energy from grid and sell it to other MGs are considered. Besides, researchers in [12] optimized the energy trading among IMGs with different RESs and loads (e.g., water pump and cooling systems). Nevertheless, none of the above methods considers battery deterioration.

For IMGs, a significant feature is their ability to recover from fault conditions with none or minimum electricity imported from the main grid, i.e., realizing self-restoration. A few research attempts dealing with IMG self-restoration during system abnormality, especially when a failure occurs on the system, have been documented in [13, 14, 5, 15], where only system economics and stability are considered on a real-time basis for an islanded IMG system. Particularly, [15] focuses on the dynamic partitioning of the distribution networks to form new MGs, whereas [14, 5] deal with the stability of the restoration process. [3,7]Researchers in [13] proposed a self-restoration process containing three steps: demand and supply information update (DSIU), target power exchange update (TPEU) which applies the consensus algorithm to allocate the power request to other MGs based on their generation capacity and decision making in self-healing (DMSH). Similar power exchange algorithm can also be found in [5]. Those research efforts, however, are not sufficient to address the intermittent nature of renewable energy and system economics and contingency options when

IMGs are grid-connected.

Aware of the necessity of developing a conditional self-restoration EMS for IMGs, in this paper, we propose an MPC-based double-layer conditional self-restoration energy management system (CSR-EMS) for both islanded and grid-connected IMGs. [1.2]Similar to [16], rolling horizon MPC with L steps ahead is applied to make the optimal decisions so as to minimize the overall operational costs within the horizon. However, only the control actions for the first step are employed, then the horizon is shifted to solve the MPC problem based on updated forecasts including load demand, RESs generation and grid price. The reason of implementing MPC is to consider operational conditions in the prediction horizon when trying to reduce the overall cost subject to a range of constraints to prevent violation of components' operating limits, e.g., ESSs charging and discharging rates and SoC limit, DG ramp-up and ramp-down rates and load switching limits. If we only consider the current step, although the resulting cost at this step may be low, in the future few steps, the costs could be unnecessarily high due to favorable operations taken in previous steps and associated constraints that prevent further cost-saving actions. Also, RES generation and grid electricity price need to be predicted ahead so as to make the most economic dispatch decisions. Main contributions of this study are summarized below:

(i) A novel two-layer CSR-EMS involving four operation steps for IMGs is proposed to achieve optimal coordinated control among wind energy, PV power, DGs, ESS and controllable loads. In this system, the mismatch between generation and demand triggers the upper layer, which receives the requested power targets and forecasts maximum guaranteed power supply (MGPS) in the prediction horizon and subsequently transmits them back to the lower layer enabling plug-and-play capability of each MG. [3.7]1.2]Comparing with other researches [13, 5] where each normal MG provides the electricity that is proportional to its generation capacity, the proposed MGPS optimally allocates the requested power based on the maximum available power at the end of the prediction horizon, considering load shedding, RESs forecast and ESSs charging/discharging

rates and SoC, to maintain the reliability of IMGs (unless all MGs completely lose power), and further protect the proprietary information as the capacities of loads and DGs are invisible for the upper layer. The aforementioned EMS is coordinated by an MPC approach which utilizes the forecast signals to dispatch DGs and arrange power exchange between IMGs with minimum cost.

(ii) [1.1]In the proposed conditional IMG self-restoration process, the abnormal MG can not only receive power support from other IMGs but also from the main grid (if connected). When the grid is connected, the proposed strategy can intelligently realize self-restoration when grid electricity price is high and grid-assisted restoration when grid price is low. When using grid power, it cannot be called self-restoration (hence conditional self-restoration). In order words, the conditionality of self-restoration is determined whether the IMG is connected to the main grid and also the time-varying grid electricity prices. This is in contrast with the existing methods where exchanging energy between MGs is the sole operation.

(iii) To enhance the reliability and accuracy of the proposed control strategy, a novel coordinated dispatch scheme for ESSs with a penalizing mechanism is devised for compensating RES fluctuations and predictions errors within the MPC. Compared with the dual ESS-wind farm proposed in [17], the new single ESS-wind-farm-based scheme has a more steady SoC of ESSs, and requires lower capital cost, a simpler control system and less maintenance.

The objective of this EMS is to minimize the total operational cost in the IMG system, which is formulated and solved in a mixed integer linear programming (MILP) with Gurobi$^{\mathrm{TM}}$. Simulation results indicate that compared to the non-predictive control method, the real-time MPC eliminates the DG output fluctuations and reduces energy consumption and aging of the ESSs. Scenarios incorporating generation deficiency and the pricing scheme show the resiliency and economical efficiency of the proposed IMG self-restoration method.

The remainder of the paper is organized as follows. In Section 2, a general description of the proposed CSR-EMS is presented. In Section 3, the lower layer control scheme is devised for normal operations, followed by Section 4 where a

real-time MPC-based conditional self-restoration scheme is detailed. A case study is carried out in Section 5. Finally, the paper concludes in Section 6.

2. General Description of the Proposed CSR-EMS

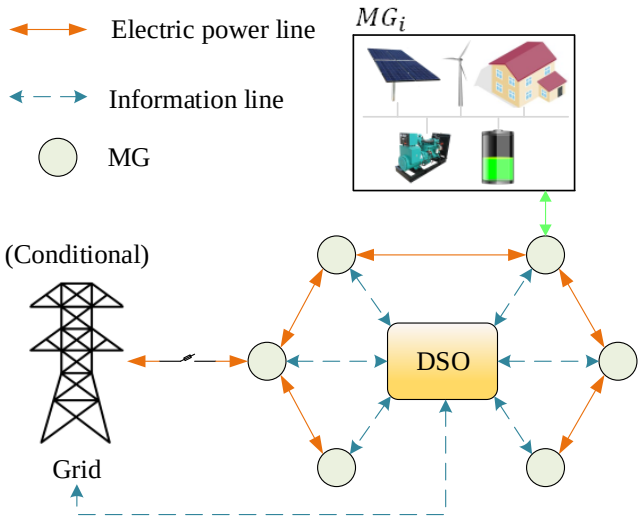

Figure 1: Architecture of the proposed IMG of interest

As shown in Fig. 1, this study focuses on an interconnected microgrid system, which can work in both islanded and grid-connected modes. Each MG contains DGs, RESs, ESSs and controllable and non-controllable loads. In order to improve the reliability of the system, each MG connects to its adjacent MGs, and the central DSO is able to communicate with all MGs and the main grid. This topology is mainly used in urban areas where the local resources are flexibly used [16]. The MG can supply sufficient power to its loads and other possible abnormal MGs. This paper emphasizes the way to recover from a fault or generation deficiency in both isolated and grid-connected modes in a cost-effective and weather-dependent manner.

The two-layer EMS can be divided into four steps, which are the demand and supply information update (DSIU), requested power exchange update (RPEU), maximum guaranteed power supply (MGPS) and decision-making process (DMP),

as shown in Fig. 2. In addition, the modules circled by orange lines indicate the upper layer. In DSIU, intelligent electronic devices (IEDs) update the generation information of DGs, SoC of ESSs, forecasted wind power, PV power and electricity price, and the data is gathered by the local EMS. A prediction horizon L is generated in the i^{th} MG at the k^{th} time instant, where the total maximum electricity provided by DGs, RESs (total denoted as $P^{G}_{i,k+j}$, $j \in \{1, 2 \cdots L\}$) and ESSs (denoted as $P^{b,\max}_{i,k+j}$) is compared with the forecasted load demand ($P^{D}_{i,k+j}$) in each step in the prediction horizon. If $P^{G}_{i,k+j} + P^{b,\max}_{i,k+j} \geq P^{D}_{i,k+j}$, in DMP, local EMS takes action considering hourly electricity price, SoC violation cost, DG generation cost and ramp-up limits, ESSs' maximum charging/discharging rates and capacities. Otherwise, the information of abnormal MGs will be sent to the upper layer to trigger the power allocation process. [3.4]The proposed CSR-EMS for IMGs works based on real-time operations; that is, when a fault or energy deficiency in a MG occurs, CSR-EMS enters conditional self-restoration and figures out the optimal power dispatch with lowest overall costs for the IMG to restore to stable operations. Also, we use real-time rolling horizon MPC to incorporate grid electricity price and renewable energy generation, which are time-varying. With different electricity price and renewable energy generation, the resulting power dispatch plan may also vary.

Once the fault locator locates the fault, normal-working MGs and abnormal MGs are denoted as N_1 and N_2 respectively. [1.1,2.8]In the self-restoration process that contains RPEU and MGPS, the abnormal MG will receive power support from other MGs under normal operation until the emergency is cleared. [2.8]For MG$_i$, $i \in N_2$, after updating available dispatchable devices, RPEU will create the requested power exchange $P^{req}_{i,k+j}$ at a particular time step k where the local EMS solves the power exchange problem based on the forecast grid electricity price (in grid-connected status), power exchange cost, and controllable load switching cost. In addition, some loads cannot be switched on/off very frequently, which incurs a switching limit within a certain period of time. Due to the fact that the fault can happen on multiple MGs, the total requested power exchange is $\psi_{k+j} = \Sigma_{i \in N_2} P^{req}_{i,k+j}$ which can be affected by the fault lo-

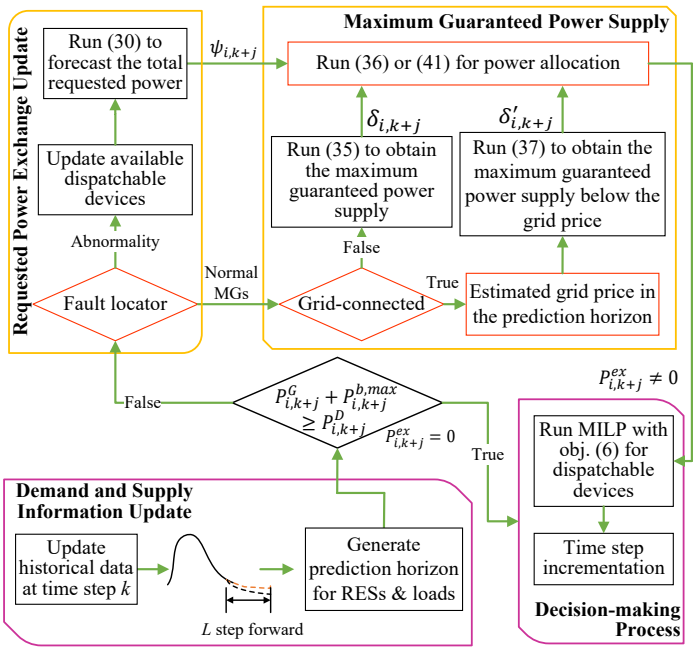

Figure 2: [2.8]Flowchart of the proposed CSR-EMS

cations to a large extent. For MG_i, $i \in N_1$ where MGPS is executed, if the grid is not connected, the maximum power that can be provided by i^{th} MG at the k^{th} step while maintaining a stable operation is obtained and denoted as $\delta_{i,k+j}$, otherwise, the maximum power supply provided below the grid price is denoted as $\delta'_{i,k+j}$. Then the target exchange power $P^{ex}_{i,k+j}$ is allocated to each normally-working MG based on ψ_{k+j} and the maximum power supply. After executing RPEU and MPGS, the target power exchange $P^{ex}_{i,k+j}$, where $j \in \mathbb{L}$ indicates the results are in a prediction horizon, is sent back to the lower layer as a load for DMP process, which realizes network resiliency and cost reduction.

3. Lower Layer Operations

[1.2]In this section, an MPC-based optimal economic dispatch formulation in the lower layer is presented. As shown in Fig. 3, at each time step k, the predictor updates the forecast data for the next L steps based on historical

information; then the MILP solver is used to obtain the estimated optimal decisions over each time step $j, j \in \mathbb{L}$, $\mathbb{L} = \{1, 2, \cdots, L\}$ in the prediction horizon with records of the previous operations; lastly, decision at time step k is applied to MGs. The performance of this real-time local EMS is greatly affected by the accuracy of forecasted PV power and wind power.

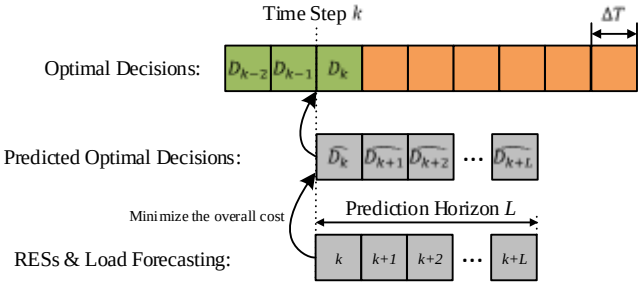

Figure 3: [1,5]MPC concept

The topology and control signal inside MG_i is demonstrated in Fig. 4. In this study, we do not consider the impact of power transmission loss and communication delay. Detailed studies for communication delay compensation can be found in [18]. The lower control layer of the proposed EMS is mainly to fulfill the following tasks: (i) predict solar and wind power generation; (ii) stabilize DG power with ESSs; (iii) optimally dispatch electric power through interaction with the main grid; and (iv) minimize the SoC deviation in the ESS.

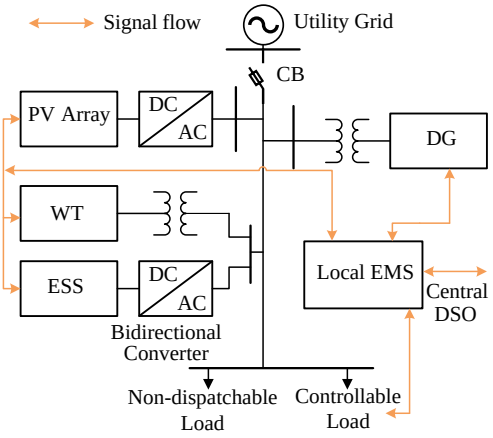

Figure 4: Schematic presentation of an MG in the IMG System

3.1. Partitioning Strategy

3.5,1.4The partitioning algorithm that produces self-sufficient MGs is applied to the distributed power system in order to reduce the complexity of rapid control and improve the reliability of the network and generation efficiency. At the lower layer, those partitioned MGs will then operate locally to ensure economic effectiveness and resiliency. For the DC IMG, we assume that for transmission/distribution lines, line resistance is much less than line reactance, and the differences among bus voltage angles are very small [19]. The partitioning algorithm is formulated as follows:

$$\min \quad \sum_{j=1}^{L}\sum_{x}(\sum_{y}\gamma_E E_{xy} + \gamma_\beta P^c_{x,j}(1-\beta^c_{x,j}) + f_x(P^{DG}_{x,j})), \tag{1}$$

$$\text{s.t.} \quad P_{x,k+j} = \sum_{y} E_{xy}|B_{xy}|(\theta_{x,k+j} - \theta_{y,k+j}), \tag{2}$$

$$\sum_{x} P^{DG}_{x,k+j} + \sum_{x}\hat{P}^{PV}_{x,k+j} + \sum_{x} P^{ref}_{x,k+j} = \sum_{x} P^{n}_{x,k+j} + P^c_{x,k+j}\cdot\beta^c_{x,k+j} \tag{3}$$

$$\theta^{min}_{x,k+j} \le \theta_{x,k+j} \le \theta^{max}_{x,k+j} \tag{4}$$

$$P^{min}_{x,k+j} \le P_{x,k+j} \le P^{max}_{x,k+j}, \tag{5}$$

where $f_x(P^{DG}_{x,j})$ is the cost function of the distributed generator at bus x, $P^c_{x,j}$ and $\beta^c_{x,j}$ are controllable loads and status of loads, respectively. $E_{xy} = 0$ means the power flow over line xy is zero, which indicates the line can be a boundary of two MGs with minimum load shedding and generation cost. Constraints (2)$\sim$(5) are power flow equations including voltage angle θ and line susceptance B. ESSs are disabled in this subsection as the focus is to produce IMGs with appropriately partitioned MGs for simulation studies.

3.2. Objective Function

The previously devised MGs are optimized locally and the objective of the local EMS/lower layer is to minimize the overall operation cost. In real-time control, the following cost function will be minimized for each MG considering ESS energy deviation penalty, DG operation cost and grid energy purchase

within a prediction horizon L: [2.6]

$$\min \quad \gamma_d d_{i,L} + \gamma_m m_{i,L} + \sum_{j=1}^{L} \left(\sum_{n \in M_i} [f_n(P_{n,j}^{DG}) + UD_{n,j}] + \gamma_{g,j} P_{i,j}^{grid} \right), \quad (6)$$

where M_i is the set of DGs inside the i^{th} microgrid. Load shedding and power exchange among MGs are not incorporated in this situation and $\gamma_d, \gamma_{g,j}, \gamma_m \geq 0$ are cost coefficients that may vary over time. Terms $d_{i,L}$ and $m_{i,L}$ are ESS and DG fluctuation penalties respectively.

3.3. DG Operating Constraints

[1.3]The cost function of a DG is assumed to be quadratically related to the output power as

$$f_n(P_{n,k}^{DG}) = a_n(P_{n,k}^{DG})^2 + b_n P_{n,k}^{DG} + c_n, \quad (7)$$

where f_n is the cost function of DG, which can be converted to a piecewise-linear function and then be solved by the MILP solver. In addition, the generation should be below certain limit, i.e., $0 \leq P_{n,k}^{DG} \leq P_n^{DG,max}$. The start up and shut down cost of the DG unit can be modeled with the auxiliary variable $UD_{n,k+j}$, $n \in M_i$, following the inequality constraints:

$$UD_{n,k+j} \geq \gamma_{SU,n}(\beta_{n,k+j}^{DG} - \beta_{n,k+j-1}^{DG}), \quad (8)$$
$$UD_{n,k+j} \geq \gamma_{SD,n}(\beta_{n,k+j-1}^{DG} - \beta_{n,k+j}^{DG}), \quad (9)$$

where $\gamma_{SU,n}$ and $\gamma_{SD,n}$ are cost coefficients for start up and shut down operations respectively, and $\beta_{n,k+j}^{DG}$ is a binary variable indicating ON(1)/OFF(0) sate of the DG. Ramp-up and ramp-down constraints are shown below.

$$P_{n,k+j}^{DG} - P_{n,k+j-1}^{DG} \leq P_{n,k+j}^{DG,max} \cdot \mu_n, \quad (10)$$
$$P_{n,k+j-1}^{DG} - P_{n,k+j}^{DG} \leq P_{n,k+j}^{DG,max} \cdot \mu_n, \quad (11)$$
$$m_{i,L} \geq \sum_{j=1}^{L} \sum_{n \in M_i} |P_{n,k+j}^{DG} - P_{n,k+j-1}^{DG}|, \quad (12)$$

where μ_n is introduced to indicate the variation of power that the DG can make in each time step. The absolute value in this equation can be formulated as two linear constraints, which can be solved by the MILP solver.

3.4. Short-term PV Power Forecast

Auto-regressive moving average (ARMA (2,1)) model is employed in this study for solar energy forecasting without exogenous input, which is denoted as $\hat{P}^{\mathrm{PV}}_{i,k+j}$ for the predicted solar energy in the i^{th} MG at the k^{th} time instant into the future j^{th} time instant in the prediction horizon. The detailed implementation of ARMA (2,1) can be found in [20]. In this study, we use real-world solar irradiance data from [21], which was collected by Dessert Knowledge Australia with one-minute resolution.

3.5. Day-ahead Wind Speed Forecasting

Accurate short-term wind speed forecasting is difficult to achieve, and in this study, we adopt the idea of coupling wind energy generators with an ESS in an MG to achieve accurate day-ahead hourly forecast [22]. We utilize the one-minute wind speed in [23], and apply ESS to make wind turbine output follow a predefined reference. Considering the humidity, temperature and historical data, WT output data under two different scenarios are forecasted with interval prediction: *pessimistic prediction* and *optimistic prediction*, which are applied from 0∼360 minutes and 720∼1080 minutes, from 360∼720 minutes and 1080∼1440 minutes, respectively. The gap between the actual electricity produced by WT output power $P^{WT}_{i,k}$ and $P^{ref}_{i,k}$ is compensated by the ESS:

$$\sigma_{i,k} = P^{ref}_{i,k} - P^{WT}_{i,k}, \tag{13}$$

where $\sigma_{i,k}$ is the part of charging/discharging rate of the ESS contributed by the WTs. Note that ESSs have other functions than stabilizing WTs output power, and therefore $\sigma_{i,k}$ is not the total charging/discharging rate of the ESS.

2.6

3.5.1. Interaction with the Grid

In this study, we only consider the cases where electricity is imported from the grid, whose amount is bounded by the following inequality,

$$0 \leq P_{i,k}^{grid} \leq P_{i,k}^{grid,max}. \tag{14}$$

The power exchange with the grid can be obtained from the power balance equation:

$$\begin{aligned} P_{i,k+j}^{grid} = P_{i,k+j}^{n} + P_{i,k+j}^{c} - P_{i,k+j}^{b} - \sum_{n \in DG_i} P_{n,k+j}^{DG} \\ - \hat{P}_{i,k+j}^{PV} - P_{i,k+j}^{ref}, \end{aligned} \tag{15}$$

where $P_{i,k+j}^{n}$ and $P_{i,k+j}^{c}$ represent critical and non-critical loads respectively. The last two terms on the left side of "=" correspond to the renewable energy forecast, and $P_{i,k+j}^{b}$ is another component of the ESS charging/discharging rate.

3.6. ESS Dynamics and Constraints

The SoC of the ESS is calculated as follows:

$$SoC_{i,k+j} = SoC_{i,k+j-1} + \Delta SoC_{i,k+j}, \tag{16}$$

$$\Delta SoC_{i,k+j} = \begin{cases} \eta^c \cdot P_{i,k+j}^{ES} \cdot \tau / EC_i & \text{if } P_{i,k+j}^{ES} < 0, \\ \eta^d \cdot P_{i,k+j}^{ES} \cdot \tau / EC_i & \text{otherwise,} \end{cases} \tag{17}$$

where η^c and η^d are the charging and discharging efficiency respectively, typically $\eta^c < 1$ and $\eta^d = \frac{1}{\eta^c}$. We denote τ as the length of one time step and EC_i as the capacity of the ESS. In addition, charging and discharging rates and SoC cannot exceed their limits, i.e.,

$$-P_i^{ES,max} \leq P_{i,k}^{ES} \leq P_i^{ES,max}, \tag{18}$$

$$SoC_i^{min} \leq SoC_{i,k} \leq SoC_i^{max}. \tag{19}$$

The output of ESS contains three elements, i.e.,

$$P_{i,k+j}^{ES} = \sigma_{i,k+j} + P_{i,k+j}^{b} + e_{i,k+j}, \tag{20}$$

where $\sigma_{i,k+j}$ and $P_{i,k+j}^{b}$ have been described in (13) and (15), $e_{i,k+j}$ is used to compensate other small forecast errors. As such, the overall function of ESS is to make $P_{i,k}^{WT}$ meet the reference power, keep the power balance and compensate forecast errors. In addition, ESS energy deviation penalty is introduced to control the storage level at the end of each MPC horizon. [1,3]The deviation variable is defined as:

$$d_{i,L} \geq \sum_{j=1}^{L} |SoC_{i,k+j} - SoC_{i,k+j-1}| + c_d |SoC_{i,k+L} - \overline{SoC}|, \tag{21}$$

where c_d is the penalty factor associated with SoC deviation, and $\overline{SoC}$ is the desired SoC level, which is set to 50% in this paper. It should be noted that setting the penalty for the battery contributes to the life cycles of ESS. To formulate equation (21) that contains absolute value into linear transformations, it is converted to the following constraints:

$$d_{i,L} \geq \sum_{j=1}^{L} (SoC_{i,k+j} - SoC_{i,k+j-1}) + c_d (SoC_{i,k+L} - \overline{SoC}), \tag{22}$$

$$d_{i,L} \geq \sum_{j=1}^{L} (SoC_{i,k+j-1} - SoC_{i,k+j}) + c_d (SoC_{i,k+L} - \overline{SoC}), \tag{23}$$

$$d_{i,L} \geq \sum_{j=1}^{L} (SoC_{i,k+j-1} - SoC_{i,k+j}) + c_d (\overline{SoC} - SoC_{i,k+L}), \tag{24}$$

$$d_{i,L} \geq \sum_{j=1}^{L} (SoC_{i,k+j} - SoC_{i,k+j-1}) + c_d (\overline{SoC} - SoC_{i,k+L}). \tag{25}$$

For demonstration, the penalty we set for SoC deviation is based on a Li-ion ESS whose cost is $\$1,000/kW$, capacity (MWh)/power (MW) ratio is 3 and the number of equivalent life cycles is 1000 [24]. Therefore, the equation below can

be derived:

$$\gamma_d d_{i,L} = Cycles \times EC_i/3, \tag{26}$$

which means the cost of battery is equal to the number of charge/discharge cycles times one third of EC_i in a prediction horizon. From (21) and (26) we can have:

$$\gamma_d \sum_{j=1}^{L} |SoC_{i,k+j} - SoC_{i,k+j-1}| \leq Cycles \times EC_i/3, \tag{27}$$

$$Cycles = \sum_{j=1}^{L} |SoC_{i,k+j} - SoC_{i,k+j-1}|/2. \tag{28}$$

By substituting (28) into (27), we can obtain

$$\gamma_d \leq EC_i/6. \tag{29}$$

4. Upper Layer Operations During Abnormality

When the central DSO receives a supply request from the lower layer, self-restoration process is initiated. The goal of self-restoration is to make the abnormal MG recover from the emergency using the power imported from selected IMGs and grid (if connected) with the minimum abnormality recovery cost. As mentioned before, two main execution steps are taken in this mode. This section details the working principles and mathematical description of the proposed CSR-EMS.

4.1. Requested Power Exchange Update

In this step, the fault locator locates the fault and the abnormal MG_i sends the requested power to the central DSO depending on the location where the circuit breaker is tripped. The objective function can be different based on the remaining generation devices. For simplicity, we only consider the worst scenario where the DGs, ESSs and WTs are tripped in one MG and the load

demand needs to be met by other MGs and PV, as described by the following formulations:

$$\min \quad \sum_{j=1}^{L}(\gamma_r P_{i,j}^{req} + \gamma_s s_{i,j}), \tag{30}$$

$$\text{s.t.} \quad P_{i,k+j}^{req} = P_{i,k+j}^{n} + P_{i,k+j}^{c} \cdot \beta_{i,k+j}^{c} - \hat{P}_{i,k+j}^{PV}, \tag{31}$$

$$0 \le P_{i,k+j}^{req} \le P_{i}^{req,max}, \tag{32}$$

$$s_{i,k+j} \ge |\beta_{i,k+j}^{c} - \beta_{i,k+j-1}^{c}|, \tag{33}$$

$$\sum_{j=-K+l}^{l} s_{i,k+j} \le s_{i}^{max}, \ \forall j, l \in \mathbb{L}, \tag{34}$$

where γ_r and γ_s are cost coefficients associated with power requested from other MGs and switching controllable loads, respectively, and $\beta_{i,k+j}^{c}$ is a binary variable indicating the status of the controllable load status. Switch action $s_{i,k+j}$ given by (33) is also penalized. Constraint (34) illustrates that the sum of switching operations in any successive K steps is restricted to be no greater than s_i^{max}. Further details on switching limits can be found in [20].

To sum up, at time step k, local EMS in abnormal MG_i generates the objective function (30) based on the fault location, the forecasted electricity price, renewable energy and load within the MPC horizon, which is subject to (31)$\sim$(34) to obtain the $P_{i,k+j}^{req}$. Due to the fact that multiple MGs may lose generation in a single fault, the total request power target is $\psi_{k+j} = \sum_{i \in N_2} P_{i,k+j}^{req}$.

4.2. Maximum Guaranteed Power Supply and Decision-making in Self-restoration

In maximum guaranteed power supply, the total requested power ψ_{k+j} in a prediction horizon at time k will be shared among normal MGs. The principle of power dispatch in the normal-working MGs are: (i) no load will be sacrificed to support the abnormal MG and (ii) the generation should be dispatched within the generator limits provided in Section 3. Therefore, the maximum power that can be provided by a normal-working MG_i is obtained by solving $\delta_{i,k}$, as shown in (35) below in an MPC horizon L, and the results are passed to the central

DSO.

$$\max \quad \sum_{j=1}^{L} \delta_{i,j} = P_{i,j}^{b} + \sum_{n \in M_i} P_{n,j}^{DG} + \hat{P}_{i,j}^{PV} + P_{i,j}^{ref} - P_{i,j}^{n} - P_{i,j}^{c}, \tag{35}$$

where the first four terms on the right-hand side denote the total generation from the normal MG and the last two terms are loads. The rest of the constraints can be found in (8)∼(13) and (16)∼(20). In general, the total power supply $\sum_{i \in N_1} \delta_{i,k}$, where N_1 indicates the normal-working MGs, is greater than the requested power ψ_k, otherwise extra power can only be provided by the grid. So far, the central DSO has received the total ψ_{k+j} from each abnormal MG and $\delta_{i,k+j}$ from normal MGs. Since prior to emergency, there is no power exchange between MGs, the power gap of the abnormal MGs is ψ_{k+j} and the power allocation process is defined as:

$$P_{i,k+j}^{ex} = \delta_{i,k+j} \cdot \frac{\psi_{k+j}}{\sum_{i \in N_1} \delta_{i,k+j}}, \tag{36}$$

where $P_{i,k+j}^{ex}$ is the exported power from MG_i at time step $k+j$. It is easy to prove that at each point in the prediction horizon $\sum_{i \in N_1} P_{i,k+j}^{ex} = \psi_{k+j}$. By applying the above power allocation strategy, the total requested power is shared fairly among normally-working IMGs.

In terms of the conditional self-restoration, the power request process is the same, but the power allocation focuses on the minimum cost. If the central DSO detects the grid is connected, it will inform the normal-working MGs where the local EMSs compare the DG cost with electricity price from the grid and solve the maximum power supply $\delta'_{i,k+j}$.

$$\max \quad \sum_{j=1}^{L} \delta'_{i,j}, \tag{37}$$

$$\text{s.t.} \quad \delta'_{i,k+j} = \sum_{n \in M_i} P_{n,k+j}^{DG} + \hat{P}_{i,k+j}^{PV} + P_{i,k+j}^{ref} - P_{i,k+j}^{n} - P_{i,k+j}^{c}, \tag{38}$$

$$\frac{f_n(P_{n,k+j}^{DG}) - f_n(P_{n,k+j-1}^{DG})}{P_{n,k+j}^{DG} - P_{n,k+j-1}^{DG}} \leq \gamma_{g,k+j}, \tag{39}$$

where the output power of ESSs cannot be included in (38) as incorporating it into $\delta'_{i,j}$ would cause instability in MGs with RESs. Equation (39), where $\gamma_{g,k+j}$ is the electricity price at time step $k+j$, ensures that the cost (\$/MWh) of generating excess power in each normal MG is no greater than the grid, and the left part of the formula can be approximate to $\frac{d}{dP}f_n(P^{DG}_{n,k+j}) = 2 \times a_n(P^{DG}_{n,k+j}) + b_n$. Therefore, equation (39) can be replaced by:

$$2a_n(P^{DG}_{n,k+j}) + b_n \leq \gamma_{g,k+j} \tag{40}$$

The rest of the constraints are identical to (7)∼(12). In this case, we can obtain the maximum power that each DG can provide below the grid electricity price, with enforced ramp limit. It is worth mentioning that if $\delta'_{i,k+j} < 0$, then $\delta'_{i,k+j} = 0$. The requested power allocation process is thus defined as:

$$P^{ex}_{i,k+j} = \begin{cases} \delta'_{i,k+j}, & \text{if } \psi_{k+j} > \sum_{i \in N_1} \delta'_{i,k+j}, \\ \delta'_{i,k+j} \dfrac{\psi_{k+j}}{\sum_{i \in N_1} \delta_{i,k+j}}, & \text{otherwise.} \end{cases} \tag{41}$$

The abnormal MG absorbs $P^{grid}_{i,k+j} = \psi_{k+j} - \sum_{i \in N_1} \delta'_{i,k+j}$ power from the grid, when the other MGs are not able to provide sufficient power economically. Therefore, the system can work either with or without the main grid, hence conditional IMG self-restoration. In this study, we only consider the cases where electricity is imported from the grid, whose amount is bounded by $P^{grid,max}_{i,k+j}$, and there is no power exportation.

The decision-making process executed in each normal MG for self-restoration includes $P^{ex}_{i,k+j}$ as a load in the power balance equation, and the following constraint must be satisfied at any step j in a prediction horizon L:

$$\begin{aligned} &P^{b}_{i,k+j} + \sum_{n \in M_i} P^{DG}_{n,k+j} + \hat{P}^{PV}_{i,k+j} + P^{ref}_{i,k+j} \\ &= P^{n}_{i,k+j} + P^{c}_{i,k+j} + P^{ex}_{i,k+j}. \end{aligned} \tag{42}$$

The whole DMP optimizes (6) subject to constraints (7)∼(12), (16)∼(21) and

(42). In this study, the constructed optimization problem comprised of two layers is solved using MILP.

5. Case Study and Simulation Results

In this section, both lower layer and the upper layer operations associated with the power allocation algorithm are demonstrated. For simulation purpose, the proposed MPC-based two-layer CSR-EMS is examined on a distributed system with six interconnected microgrids as shown in Fig. 5 which is modified from the IEEE standard 68-bus test system with partitioning methods in [25], where each MG contains a certain number of RESs, DGs, ESSs and controllable loads. The cost of DGs and the capacity of ESSs are taken from [13]. We assume that each MG contains one ESS and at least one DG and that all MGs have sufficient capacity to supply their own loads during normal operations.

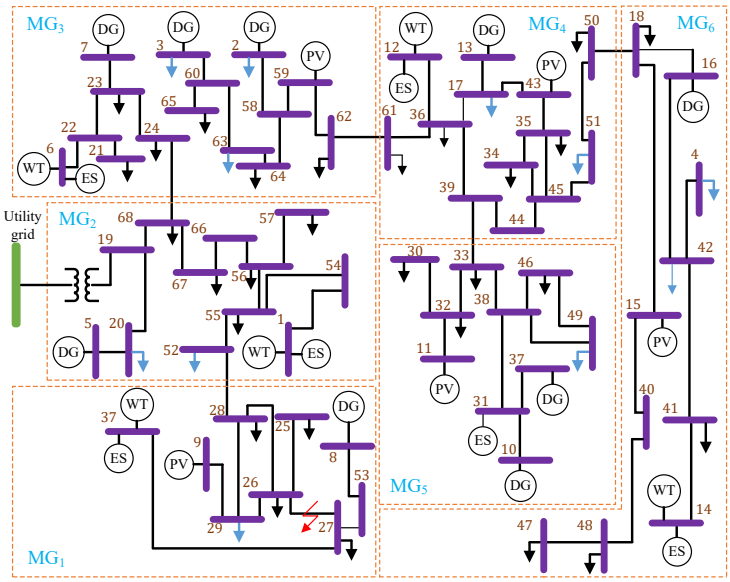

Figure 5: [3.6]Interconnected microgrid system of interest

Table 1: The capacitance and location of the components in each MG

MG_i	Type	Bus	$P^{cap}(MW)$
MG_1	DG	8	4
	WT	37	1
	PV	9	1
	ES	37	2
	Load	25∼29	3(n), 2(c)
MG_2	DG	5	8
	WT	1	3
	ES	1	2
	Load	20, 52, 55∼57, 67, 68	6(n), 2(c)
MG_3	DG	7, 3, 2	4, 6, 4
	WT	6	2
	PV	59	1
	ES	6	2
	Load	21, 23, 24, 62∼65	10(n), 3(c)
MG_4	DG	13	8
	WT	12	2
	PV	43	1.5
	ES	12	2
	Load	17, 34∼36, 50, 51, 61	8(n), 2(c)
MG_5	DG	10,37	2, 4
	PV	11	1.5
	ES	31	2
	Load	32, 33, 46, 49	5(n), 2(c)
MG_6	DG	16	8
	WT	14	1
	PV	15	1
	ES	14	2
	Load	18, 41, 42, 47, 48	3(n), 2(c)

5.1. Energy Forecasting

Fig. 6 illustrates the PV power output during one-day period with one-minute resolution and its prediction results using ARMA(2,1) model. At each time step, the output power from solar PV is predicted for the next 7 minutes. The data from [21] contains $1,440 \times 7 = 10,080$ one-minute data for seven days. In this case, the first 6 days' data are used to train the ARMA model, and the model is tested on the 7^{th} day. TABLE 2 shows that the prediction error is below 3.1%, which is applicable for real-time optimization.

As mentioned before, we use the day-ahead hourly prediction to forecast wind power generation that contains both optimistic and pessimistic forecasts. The one-minute wind speed data are adopted from [23]. Fig. 7 depicts the predicted and referenced wind power available to the WT MPPT algorithm

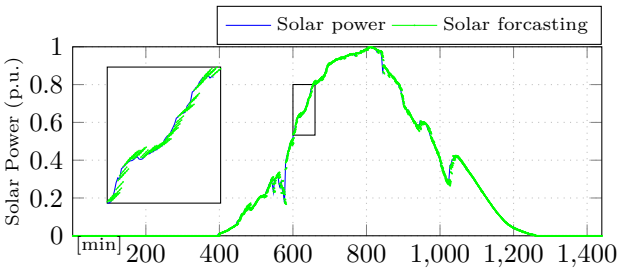

Figure 6: Short-term PV power prediction

Table 2: Average prediction MAE for solar energy (%)

Step	1	2	3	4	5	6	7
Train-ning	0.7908	1.2023	1.5955	1.9760	2.3341	2.6794	3.0326
Test	0.8330	1.2965	1.6534	2.0156	2.3917	2.7623	3.0901

during a 1440-minute period. In this case, the fluctuation degree value (FDV): $FDV = \frac{1}{T}\sum_{k=1}^{T}\sqrt{(P_{i,k}^{ref} - P_{i,k}^{WT})^2}$ is 1.7×10^{-3} and ESS ensures the wind farm output follows $P_{i,k}^{ref}$. Though WT power is forecasted on a day-ahead basis, we still only use the results in the prediction horizon at each step, which is 7 minutes.

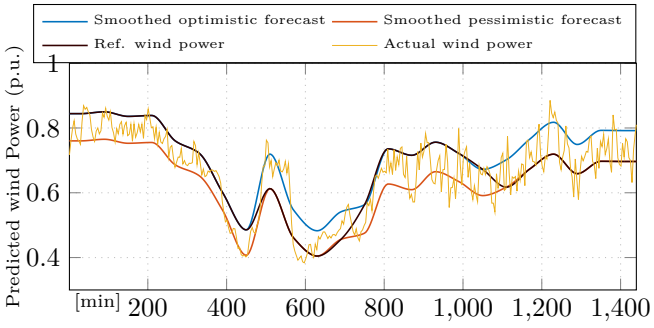

Figure 7: Day-ahead wind forecast

5.2. Real-time Control in Normal Operation Mode

In this case study, each MG works independently to optimally dispatch the DERs by using (6)∼(42) and no load switching is allowed. [2.7]According to (29),

γ_d is less than $EC_i/6$ which is $2(MW)/6$ in this paper. In addition, for one-minute resolution the result should be multiplied by 60s, which is $(2/6 \times 60 =)$ 20. In this paper, γ_d is set to be 10 and γ_m should be higher, which is 15, to mitigate the fluctuation of DGs, whereas $\gamma_{g,j}$ $(j \in \mathbb{L})$ is the electricity price. In this paper, $P_n^{DG,min}$ is set to be 10% of $P_n^{DG,max}$, and SoC_i^{max} and SoC_i^{min} are 0.9 and 0.15 respectively. The charging efficiency η^c is 0.95. All the initial points for dispatchable units are set to be 0.5 of their maximum values. All the above values are applied from 00:01∼24:00 in a one-day period with one-minute resolution. High DG power output ripple is noticeable in the presence of MPC

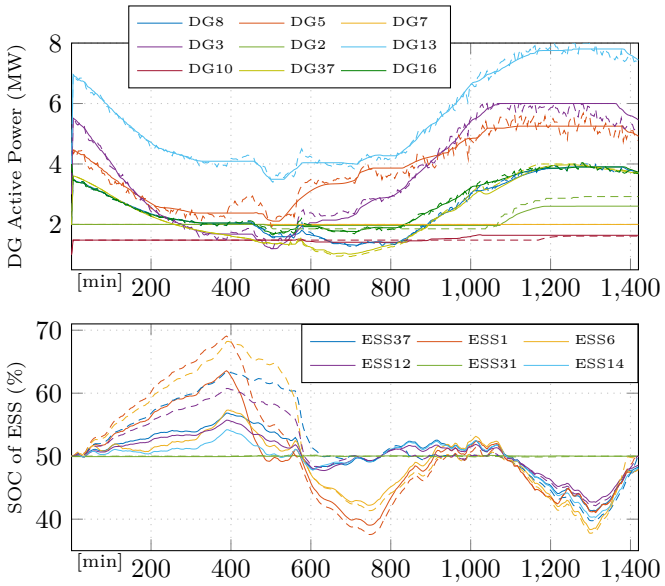

Figure 8: Normal period: proposed 7-step MPC-EMS (solid) and EMS without using MPC (dashed)

in Fig. 8 where the optimal schedules of DGs and ESSs are displayed with the solid lines representing the dispatch result when MPC and RESs scheduling are applied. It is obvious that without prediction, the power exported from DGs fluctuates due to the intermittency of RESs and ESSs not being utilized to compensate RES variation, which reduces the reliability of the IMGs and could potentially cause power outages. Detailed numerical results, corresponding to Fig. 8 for normal operation mode, can be found in TABLE 3 (scenarios 1 and

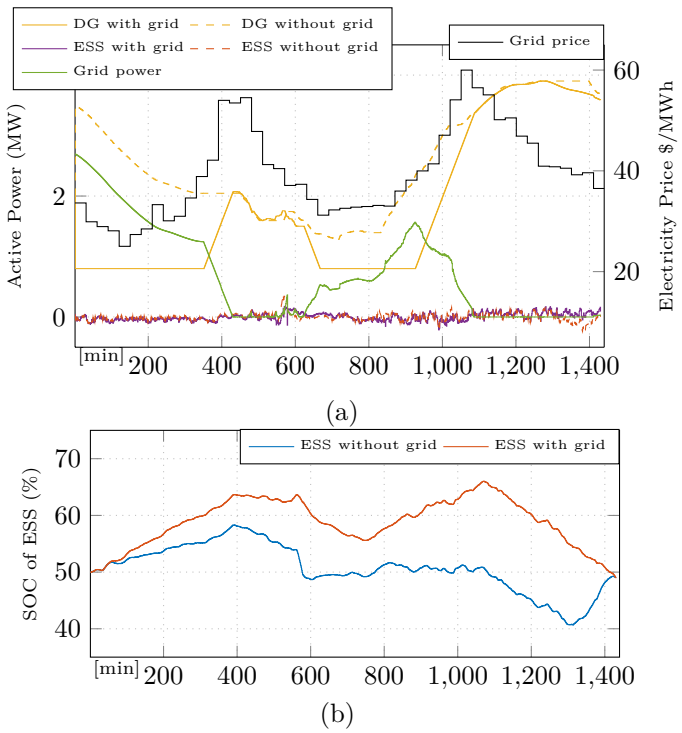

Figure 9: [2.5]Normal period: (a) MPC based resources dispatch in MG_1, (b) ESSs schedule in MG_1

2). To evaluate the performance of the ESSs, ESS aging is modeled through computing equivalent charge-discharge full cycles (EFC) [26]. [2.5]In this study, we propose a daily equivalent charge-discharge full cycles (DEFC) with one-minute resolution: $DEFC = \frac{1}{2C_i}\sum_{k=1}^{T}|P_{i,k}^{ES}(k)|$ where C_i is the capacity of ESS in the i^{th} MG. Obviously, the islanded IMG system with 7-step MPC requires less total generation and less DEFC due to optimal use of ESSs, as the charging/discharging efficiencies of ESSs are not equal to 1. By applying MPC,

Table 3: [2.8,2.5]Numerical results (N: normal, A: abnormality, energy in MWh)

No.	Mode	MPC	Grid	DG Gen.	DEFC of ESSs |Energy exchange of MGs						Grid import	CSR.$	Tot.$
					MG_1	MG_2	MG_3	MG_4	MG_5	MG_6			
1	N	No	No	618.53	0.34|nil	0.52|nil	0.48|nil	0.28|nil	0.02|nil	0.35|nil	nil	nil	25028
2	N	7-step	No	612.81	0.29|nil	0.49|nil	0.38|nil	0.23|nil	0.02|nil	0.28|nil	nil	nil	24549
3	N	7-step	Yes	551.57	0.36|nil	0.49|nil	0.47|nil	0.26|nil	0.01|nil	0.30|nil	65.19	nil	23848
4	A	7-step	No	611.28	0.27|+2.56	0.48|-0.40	0.39|-0.68	0.24|-0.56	0.03|-0.60	0.29|-0.32	nil	103	24652
5	A	7-step	Yes	611.28	0.27|+2.56	0.47|0.00	0.39|-0.61	0.24|0.00	0.03|-0.49	0.31|-1.06	**0.42**	**80**	**24629**

the ESS can make the wind turbine output follow the reference power to eliminate the fluctuation of DGs caused by the intermittent wind. The continuous changes on the SoCs of ESSs are caused by two factors: (i) reference wind power is switching between pessimistic and optimistic prediction and (ii) the $\overline{SoC}$ in (21) is set to be 50% which makes SoC fluctuate around 50%. [3.5]Computationally, a maximum calculation time of 0.018s for one iteration is applicable for the normal operation with one-minute dispatch.

[2.5]The real-time one-minute electricity price is obtained and modified from [27]. Fig. 9 is the optimal economic dispatch of MG_1 in grid-connected mode. In Fig. 9 (a), MG_1 absorbs the energy from the grid at a low price, while as the price grows, the power imported from the grid starts to decrease. Fig. 9 (b) illustrates that DEFC is affected by the added grid as ESSs will store energy when the grid price is low, whereas the SoC remains to be 50% at the end. According to scenario 3 in TABLE 3, the cost is reduced when importing electricity from the utility grid at low prices.

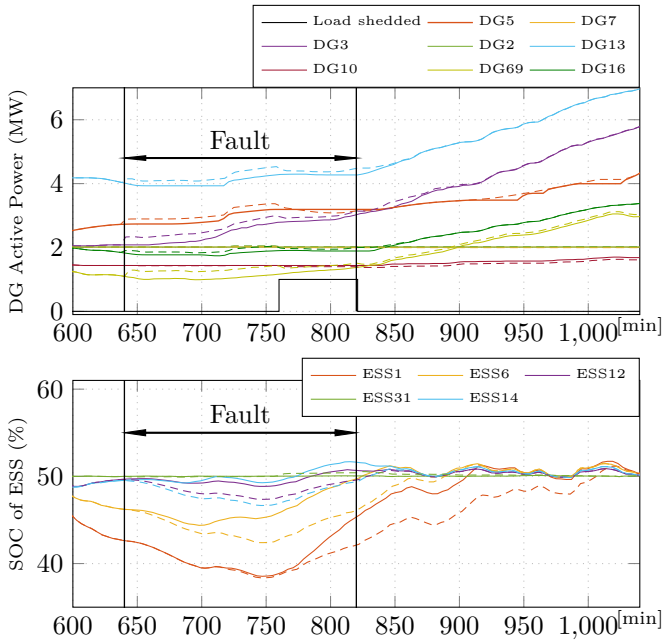

Figure 10: DER dispatch in normal period (solid) and abnormal period (dashed), both with MPC and RES scheduling

5.3. Real-time Control during Abnormal Periods

[2.7]In this subsection, a single fault is introduced in the IMG system in MG_1 between bus 26 and 27 when $t = 640$ minutes, which is recovered when $t = 820$ minutes. Terms γ_s and γ_r in Section 4 are set to 10 and 10.8, respectively. As mentioned before, we consider the worst-case scenario, i.e., when the fault happens, all other DERs (including ESS37) in the MG are tripped for self protection, and PV power is the only available energy source. The total load demand of the MG_1 is 3.01MW. In order to support the load, the on-emergency MG needs 2.561 MWh electricity from other normal-working MGs during the 180-minute fault period. The dynamic power allocation for each MG is obtained by solving the centralized optimization problem discussed in Section 4.2.

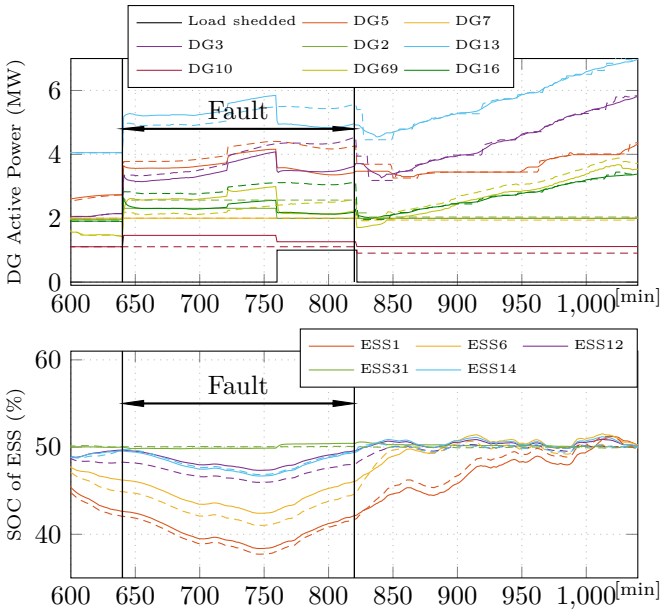

Figure 11: [3.7]Abnormal period: proposed MGPS process (solid) and the TPEU in [13] i.e., no maximum guaranteed power supply (dashed)

Fig. 10 demonstrates the re-dispatch results of DGs and ESSs during the fault period. DG5 and ESS1 require the longest restoration time, while the DEFC of ESS1 is not much affected. We can see that the controllable loads in MG_1 are switched off between $t = 760$ minutes to $t = 820$ minutes due

to (30), and the total load shedding energy is 1.03 MWh, with loads in other MGs intact. [2.5]Scenario 4 in TABLE 3 shows the numerical results during this self-restoration process, where the total generation decreases because of load shedding and the isolated loads caused by the fault. Power exchange from MG_1 is the requested power supplied collectively by the rest of MGs, and the power allocation is fair and matches the request. The allocated power is not related to the capacity of DGs (e.g., MG_4 and MG_5), but to the maximum power that an MG can supply in the prediction horizon considering all constraints. Although ESSs discharge faster during the fault, their average DEFCs are not affected, which remain around 0.28s. [3.5]Computationally, a maximum calculation time of 0.031s for one iteration is viable for the self-restoration with a one-minute dispatch.

Table 4: [2.8]IMG restoration cost ($)

Fault scale	1	2	3	4	5
MGPS	102.9	103.6	104.5	106.1	110.5
TPEU in [13]	109.1	110.1	111.3	115.0	120.9

[3.7]The comparison between the dispatch result with MGPS in the proposed CSR-EMS and the power allocation method in [13] is depicted in Fig. 11, where the requested power for the on-emergency MG (MG_1) is increased by 5 times to emulate the IMG system fault. Simulations have shown that the IMG becomes unstable when the requested power increases by 5.7 times with the existing method, whereas the proposed CSR-EMS ensures system reliability when fault power increases by 9.4 times, which verifies that the power sharing method in MGPS is more reliable. The self-restoration cost is recorded in TABLE 4, where "fault scale" $(1, 2, \cdots 5)$ represents the power requested by MG_1, in multitudes of the power requested by MG_1 in Fig 5. It can be seen that the proposed CSR-EMS always has a lower recovery cost than the method in [13].

Fig. 12 shows the real-time one-minute electricity price used in this study, which is adopted from [27]. Fig. 13 compares self-restoration process and grid-assisted restoration, and demonstrates that the grid can play an active role in

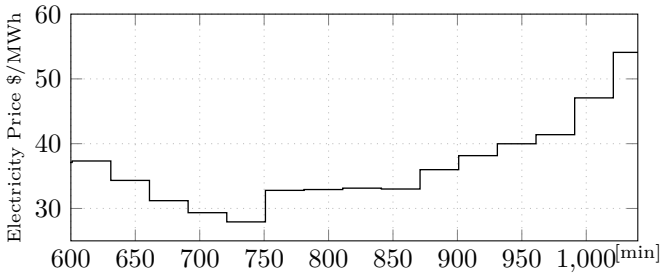

Figure 12: Grid electricity price

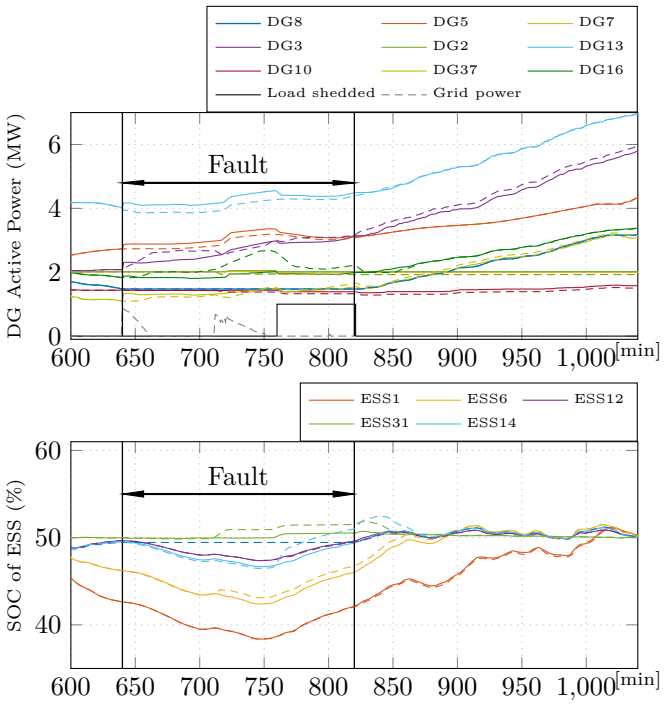

Figure 13: Conditional self-restoration mode with gird (dashed) and without grid (solid)

supporting the on-emergency MG. It can be observed that as the grid electricity price varies, the CSR-EMS will automatically use available power inside IMGs and import energy from the grid, for optimal economic benefits. When connected to the grid, DEFCs of ESSs are not much affected; however, DGs are dispatched differently, the central DSO reduces the power exported from MGs that contain high-cost DGs and increases power allocation from low-cost MGs

and main grid. Numerically, from TABLE 3 we can see that with the proposed CSR-EMS, the IMG system is able to intelligently draw 0.42 MWh electricity from the grid, with $22.3\% = (103 - 80)/103 \times 100\%$ (see TABLE 3) less fault recovery cost (i.e., CSR.$) than using energy solely from off-emergency IMGs, showing greatly increased economic benefits.

6. Conclusions

In this study, we have proposed an MPC-based two-layer four-step conditional self-restoration EMS for IMG systems. A comprehensive comparison study was conducted, which has demonstrated that real-time 7-step MPC is able to eliminate RESs' fluctuations and diminish the daily equivalent charge-discharge full cycles of MG ESSs, compared to existing research. Furthermore, the proposed CSR-EMS can automatically utilize low-cost electricity from IMGs and the main grid, so as to optimize economic benefit of the IMG system in faulty conditions, while maintaining load-demand balance, so as to achieve conditional self-restoration during IMG abnormalities. Future work will involve battery sizing and development of a hierarchical decision-making process for priority-based IMG conditional self-restoration to accommodate prediction inaccuracies and reduce capacity/power ratio of ESSs.

7. References

References

[1] K. Baldwin, A. Blakers, M. Stocks, At its current rate, australia is on track for 50% renewable electricity in 2025 (May 2019).
URL `http://theconversation.com`

[2] Q. Zhou, M. Shahidehpour, A. Alabdulwahab, A. Abusorrah, Flexible division and unification control strategies for resilience enhancement in networked microgrids, IEEE Trans. on Power Systems 35 (1) (2019) 474–486.

[3] Ieee guide for design, operation, and integration of distributed resource island systems with electric power systems, IEEE Std 1547.4-2011 (2011) 1–54.

[4] M. N. Alam, S. Chakrabarti, A. Ghosh, Networked microgrids: State-of-the-art and future perspectives, IEEE Trans. on Industrial Informatics 15 (3) (2018) 1238–1250.

[5] X. Wu, Y. Xu, X. Wu, J. He, J. M. Guerrero, C.-C. Liu, K. P. Schneider, D. T. Ton, A two-layer distributed cooperative control method for islanded networked microgrid systems, IEEE Trans. on Smart Grid 11 (2) (2019) 942–957.

[6] Z. Liu, L. Wang, L. Ma, A transactive energy framework for coordinated energy management of networked microgrids with distributionally robust optimization, IEEE Trans. on Power Systems 35 (1) (2019) 395–404.

[7] H. Guo, S. S. Yu, H. H. Iu, T. Fernando, C. Zheng, A complex network theory analytical approach to power system cascading failurefrom a cyber-physical perspective, Chaos: An Interdisciplinary Journal of Nonlinear Science 29 (5) (2019) 053111.

[8] M. Saleh, Y. Esa, A. Mohamed, Applications of complex network analysis in electric power systems, Energies 11 (6) (2018) 1381.

[9] W. Sun, S. Ma, I. Alvarez-Fernandez, A. Golshani, et al., Optimal self-healing strategy for microgrid islanding, IET Smart Grid 1 (4) (2018) 143–150.

[10] A. M. Jadhav, N. R. Patne, Priority-based energy scheduling in a smart distributed network with multiple microgrids, IEEE Trans. on Industrial Informatics 13 (6) (2017) 3134–3143.

[11] R. Lahon, C. P. Gupta, E. Fernandez, Priority-based scheduling of energy exchanges between cooperative microgrids in risk-averse environment, IEEE Systems Journal 14 (1) (2019) 1098–1108.

[12] A. Ouammi, Y. Achour, D. Zejli, H. Dagdougui, Supervisory model predictive control for optimal energy management of networked smart greenhouses integrated microgrid, IEEE Trans. on Automation Science and Engineering 17 (1) (2019) 117–128.

[13] Z. Wang, B. Chen, J. Wang, C. Chen, Networked microgrids for self-healing power systems, IEEE Trans. on Smart Grid 7 (1) (2015) 310–319.

[14] T. Ding, Z. Wang, W. Jia, B. Chen, C. Chen, M. Shahidehpour, Multi-period distribution system restoration with routing repair crews, mobile electric vehicles, and soft-open-point networked microgrids, IEEE Trans. on Smart Grid.

[15] X. Cao, J. Wang, J. Wang, B. Zeng, A risk-averse conic model for networked microgrids planning with reconfiguration and reorganizations, IEEE Trans. on Smart Grid 11 (1) (2019) 696–709.

[16] A. Parisio, C. Wiezorek, T. Kyntäjä, J. Elo, K. Strunz, K. H. Johansson, Cooperative MPC-based energy management for networked microgrids, IEEE Trans. on Smart Grid 8 (6) (2017) 3066–3074.

[17] C.-L. Nguyen, H.-H. Lee, A novel dual-battery energy storage system for wind power applications, IEEE Trans. on Industrial Electronics 63 (10) (2016) 6136–6147.

[18] S. S. Yu, T. K. Chau, T. Fernando, H. H.-C. Iu, An enhanced adaptive phasor power oscillation damping approach with latency compensation for modern power systems, IEEE Trans. on Power Systems 33 (4) (2017) 4285–4296.

[19] H. Seifi, M. S. Sepasian, Electric power system planning: issues, algorithms and solutions, Springer Science & Business Media, 2011.

[20] T. K. Chau, S. S. Yu, T. Fernando, H. H.-C. Iu, Demand-side regulation provision from industrial loads integrated with solar pv panels and energy

storage system for ancillary services, IEEE Trans. on Industrial Informatics 14 (11) (2017) 5038–5049.

[21] Historical data — DKA solar centre (July 2019).
URL http://dkasolarcentre.com.au/historical-data

[22] A. Giannitrapani, S. Paoletti, A. Vicino, D. Zarrilli, Bidding wind energy exploiting wind speed forecasts, IEEE Trans. on Power Systems 31 (4) (2015) 2647–2656.

[23] Akrherz, Iem asos one-minute data download (July 2019).
URL https://mesonet.agron.iastate.edu

[24] N. DiOrio, A. Dobos, S. Janzou, Economic analysis case studies of battery energy storage with SAM, Tech. rep., National Renewable Energy Lab.(NREL), Golden, CO (United States) (2015).

[25] R. A. Osama, A. F. Zobaa, A. Y. Abdelaziz, A planning framework for optimal partitioning of distribution networks into microgrids, IEEE Systems Journal 14 (1) (2019) 916–926.

[26] A. Berrueta, M. Heck, M. Jantsch, A. Ursúa, P. Sanchis, Combined dynamic programming and region-elimination technique algorithm for optimal sizing and management of lithium-ion batteries for photovoltaic plants, Applied energy 228 (2018) 1–11.

[27] National-electricity-market-nem (September 2019).
URL https://www.aemo.com.au/Electricity/National-Electricity-Market-NEM